Artificial neural network modeling of scale-dependent dynamic capillary pressure effects in two-phase flow in porous media

Luqman K. Abidoye and Diganta B. Das

ABSTRACT

A computationally efficient and simple alternative platform for the prediction of the domain scale dependence of the dynamic capillary pressure effects, defined in terms of a coefficient named as dynamic coefficient (τ), is developed using an artificial neural network (ANN). The input parameters consist of the phase saturation, media permeability, capillary entry pressure, viscosity ratio, density ratio, temperature, pore size distribution index, porosity and domain volume with corresponding output τ obtained at different domain scales. Different ANN configurations as well as linear and nonlinear multivariate regression models were tested using a number of performance criteria. Findings in this work showed that the ANN structures with double hidden layers perform better than those with a single hidden layer. In particular, the ANN configuration with 13 and 15 neurons in the first and second hidden layers, respectively, performed the best. Using this best-performing ANN, effects of increased domain size were predicted for three separate experimental results obtained from literature and our laboratory with different domain scales. Results showed increased magnitude of τ as the domain size increases for all the independent experimental data considered. This work shows the applicability and techniques of using ANNs in the prediction of scale dependence of two-phase flow parameters.

Key words | ANN, dynamic capillary pressure effects, multi-scale, porous media, two-phase flow, viscosity ratio

Luqman K. Abidoye
Diganta B. Das (corresponding author)
Chemical Engineering Department,
Loughborough University,
Loughborough,
Leicestershire LE11 3TU,
UK
E-mail: *d.b.das@lboro.ac.uk*

INTRODUCTION

Characterizing single and two-phase flow in porous media is of particular interest in issues relating to remediation of contaminant, oil recovery, flow in pulp and paper systems, geological sequestration of CO_2, and others (Ingham & Pop 2005; Hill *et al.* 2007; Kobayashi *et al.* 2008; Bear 2013; Abidoye & Das 2015; Das *et al.* 2014). The topic of the paper, namely, the two-phase flow behavior in porous medium can be macroscopically described by the equations for conservation of fluids' mass and momentum (Kalaydjian 1987); however, these should be coupled with constitutive relationships among capillary pressure (P^c) saturation (S) and relative permeability (K_r) (Abidoye & Das 2015; Khudaida & Das 2014). The traditional approaches for determining the P^c–S–K_r relationships assume that the flow parameters are functions of steady-state saturation, i.e., when $dS/dt = 0$. For example, the definition of P^c according to the Laplace law ($P^c = 2\gamma \cos\theta / r$) is valid under static conditions (Kalaydjian 1992) where γ is the interfacial tension between the two fluids and θ is the contact angle. As evident, the law defines P^c to be a function of contact angle (θ) which, in turn, depends on the physical properties of the fluids and the porous medium (e.g., wettability (Dullien *et al.* 1990) and viscosity ratio (Danish & Jacquin 1983)) that are in contact with one another. Despite these notions, the saturation-rate (dS/dt) dependency of the P^c–S relationships has been observed in many studies during

doi: 10.2166/hydro.2014.079

dynamic two-phase flow in porous media which is referred to as the dynamic capillary pressure effect (Hassanizadeh *et al.* 2002; Mirzaei & Das 2007).

A large number of papers involving numerical simulations and experiments concerning the dynamic P^c–S relationship have been published (see, e.g., Topp *et al.* 1967; Smiles *et al.* 1971; Stauffer 1978; Kalaydjian 1992; Wildenschild *et al.* 2001; Hassanizadeh *et al.* 2002; O'Carroll *et al.* 2005a, 2005b; Oung *et al.* 2005; Camps-Roach *et al.* 2010; Sakaki *et al.* 2010; Goel & O'Carroll 2011; Das & Mirzaei 2012; Diamantopoulos & Durner 2012; Das & Mirzaei 2013; Khudaida & Das 2014). Particularly, the studies by Kalaydjian (1992) and Hassanizadeh & Gray (1993) identified the dependence of the P^c on saturation (S) and the rate of change of saturation ($\partial S/\partial t$). This is defined as the 'dynamic capillary pressure effect' and it is quantitatively described by a proportionality constant term τ known as the dynamic coefficient. In the last couple of decades, attempts have been made to incorporate this term in the traditional mathematical definition for the two-phase systems as expressed in Equation (1) to account for the difference in the P^c–S relationships under the dynamic and static flow conditions

$$P^{c,dyn} - P^{c,static} = -\tau\left(\frac{\partial S}{\partial t}\right) \tag{1}$$

where $P^{c,dyn}$ [kg·m^{-1}·s^{-2}] is the phase pressure difference (P_{nw}–P_w) measured under dynamic or non-equilibrium condition, $P^{c,static}$ [kg·m^{-1}·s^{-2}] is the capillary pressure measured under equilibrium condition, $\partial S/\partial t$ [s^{-1}] is the rate of saturation change, and τ [kg·m^{-1}·s^{-1}] is the dynamic coefficient as mentioned earlier. P_w and P_{nw} are the pressures of the wetting and non-wetting phases, respectively, at the interface between the two phases.

As explained by Das *et al.* (2007), the magnitude of τ relates to how close or far from capillary equilibrium ($\partial S/\partial t = 0$) the two-phase flow system is. However, its magnitude is reported to be dependent on the size of the domain (Dahle *et al.* 2005; Camps-Roach *et al.* 2010; Bottero *et al.* 2011a, 2011b; Das & Mirzaei 2012; Das & Mirzaei 2013) apart from other factors, e.g., fluid viscosity and density ratios (Gielen *et al.* 2005; Das *et al.* 2007; Goel & O'Carroll 2011; Joekar-Niasar & Hassanizadeh 2011), permeability of the medium (Camps-Roach *et al.* 2010; Tian *et al.* 2012; Hanspal *et al.* 2013) and heterogeneities (Manthey *et al.* 2005; Das *et al.* 2006; Das & Mirzaei 2013; Mirzaei & Das 2013). This paper is specifically concerned with the domain scale effects on the dynamic coefficient (τ) as discussed below.

Understanding the influence of domain scale on the magnitude of τ is important as the two-phase flow can occur in porous domains at pore, core and/or larger field scales. Previous experimental (Bottero *et al.* 2011b) and numerical (Dahle *et al.* 2005) studies showed an increasing magnitude of τ as the domain size increases. However, some authors have expressed different conclusions about the effect of domain size on τ. Camps-Roach *et al.* (2010) and Das & Mirzaei (2012, 2013) do not find significant difference between the locally measured and the upscaled value of τ. This indicates the possible inconsistency surrounding the exact trend of the magnitude of τ with the domain scale.

Meanwhile, investigating the dynamic capillary pressure effects on two-phase flow systems in porous media often requires time-consuming experiments and/or cost-intensive modeling and simulations, which generally involve complex procedures to set up and run the simulations (Spalding 1981; Hanspal *et al.* 2013; Khudaida & Das 2014). Furthermore, determining the effects of domain scale on τ also imposes further challenges with the implications of various averaging techniques which are proposed and applied in the literature. For example, Bottero *et al.* (2011a) proposed the centroid-corrected averaging method as the most appropriate for two-phase systems while authors such as Das & Mirzaei (2012, 2013), Camps-Roach *et al.* (2010) and Manthey *et al.* (2005) employed different averaging techniques to determine the scale dependency of τ. While the scale dependency of τ continues to be a topic of discussion, there is an obvious lack of industrially relevant, easy to use, tools that can easily determine these behaviors. To address these challenges/issues, we wish to investigate the domain scale effect on τ using alternative platforms offering less complex and fast implementation procedures to achieve the same end. As such, a computationally economical and simpler platform for investigating the effects of domain scale on τ is presented using an artificial neural network (ANN).

Indeed, the ANN is a powerful modeling tool with the ability to learn and generalize functions from rounds of training as well as extract essential information from data

(Wang & Fu 2008; Khashei & Bijari 2013). It provides a novel, elegant and valuable class of computational tools for data analysis and prediction (White 1989; Deka & Quddus 2014). Its building blocks or the elements are the 'neurons' which are grouped into input, hidden and output layers with respective biases, weights and transfer functions (Mueller & Hemond 2013; Yurdakul & Akdas 2013). The network manipulates the values of the biases and weights in a sequence of training processes and uses the transfer functions to establish the relationships between the inputs and the outputs. It has found applications in wide areas of science and engineering problems including medical fields to illustrate medical diagnosis (Amato *et al.* 2013), renewable energy systems, economics, psychology and many more (Kalogirou 2000).

Although the modeling parameters involved in the two-phase flow in porous media are interrelated in a complex manner, it has been shown that an ANN can approximate the relevant functions to the desired accuracy (Zhang *et al.* 1998; Hanspal *et al.* 2013; Das *et al.* 2015). This quality of the ANN can, thus, be harnessed to investigate the complex behavior of two-phase flow in porous media. For example, please see the works on the application of the ANN to study two-phase flow pattern (Mehta *et al.* 2013), oil flow rate (Ahmadi *et al.* 2013), groundwater contamination and pollutant infiltration forecasting (El Tabach *et al.* 2007), optimization of groundwater remediation problems (Rogers & Dowla 1994; Johnson & Rogers 2000), large-scale water resource management (Yan & Minsker 2006; Mounce *et al.* 2014), and permeability modeling in petroleum reservoir management (Karimpouli *et al.* 2010). Recently, Hanspal *et al.* (2013) demonstrated the effectiveness of an ANN in the determination of dynamic effects in a two-phase flow system, though they did not investigate the effect of domain scale on τ. They concluded that a well-trained and validated ANN structure can give reliable prediction of τ in a two-phase flow system. In addition to being inexpensive, an ANN offers a faster alternative to modeling of a complex system with the freedom from excessive imposition of constraints on the complex relationships between the input and output variables. Thus, our work explores the above qualities of the ANN to investigate the domain scale dependency of τ in the two-phase flow system in porous media.

MODELING APPROACHES

ANN and multivariate regression (MVR) techniques were used to investigate the domain scale dependency of the τ in the two-phase flow system. The MVR was chosen because of the ease of implementation and to provide an alternative approach to compare different ANN configurations against.

Artificial neural network

For successful modeling of dynamic two-phase flow behavior using an ANN, the impacts of the network configuration, training and evaluation procedures cannot be overemphasized. In this work, different network configurations were investigated using a feed forward network. This is the commonest network in engineering application (Kalogirou 2000; Deka & Quddus 2014). For the purpose of training, a back-propagation algorithm was employed. Details of the configurations, training and data processing are discussed below.

Data sources and pre-processing

In this paper, the literature data were obtained from the results by Das *et al.* (2007), Mirzaei & Das (2007), Goel & O'Carroll (2011), Das & Mirzaei (2012) and Hanspal & Das (2012) and additional data (Abidoye & Das 2015) from in-house laboratory experiments using methodology described by Das & Mirzaei (2012). Nine independent variables that have been identified as important in the literature were used as input variables in the simulations. These include, water saturation (S), media permeability (k), capillary entry pressure (P_d), fluid viscosity ratio (μ_r) defined as the ratio of the non-wetting phase viscosity (μ_{nw}) to that of the wetting phase viscosity (μ_w), fluid density ratio (D_r) defined as the ratio of the non-wetting phase density (D_{nw}) to that of the wetting phase density (D_w), temperature (T), pore size distribution index (λ), porosity (ϕ), and domain volume (V). The output variable is the corresponding τ. The number of data points under each variable is 307. In selecting these data sources, efforts were made to ensure that the data contain varying experimental or simulation parameters and conditions needed

to fulfill the objective of this paper. For example, the works of Mirzaei & Das (2007), Goel & O'Carroll (2011), Das & Mirzaei (2012) and Hanspal & Das (2012) were conducted using different domain volumes. Furthermore, our laboratory experiments (Abidoye & Das 2015) were conducted for different heights of domain (4, 8 and 12 cm height) but with the same diameter for 500 cSt viscosity ratio of silicone–oil water system. These features enhance the training of the ANN to easily capture the nonlinear relationships between the domain size and τ. Important statistics of the variables are listed in Table 1.

Compared to the number of data points commonly required to plot a complete $\tau - S$ curve (typically less than 10 data points, see, e.g., Bottero *et al.* (2011b)), the amount of data used in this work (>300 data points) is over 30 times more than what is typically required. Also, this work employs a simple ANN structure. These features ensure that artificial over-fitting of the data is avoided. Complex ANN structures and few data can lead to artificial over-fitting in ANN modeling (Hanspal *et al.* 2013).

ANN development

Various configurations of ANN were developed and tested to determine the most suitable network. The configuration approach followed that demonstrated in Hanspal *et al.* (2013) as proposed by Srinivasulu & Jain (2006). The ANNs include single and double hidden layers. A program file with lines of code was written and implemented in MATLAB to create, train, validate and test the networks as well as to generate the goodness of fit of the parameters, e.g. correlation coefficients and slope for the predicted output (τ). The developed networks consist of different layers comprising the input, hidden and the output layers. The input layer is occupied by the independent variables while the output layer is for the dependent variable. The hidden layer is occupied by the neurons which are the constitutive units that receive the input and operate on them to produce the output. The code divides the data set randomly into 60, 20 and 20% corresponding to the data for training, validation and testing, respectively. As stated before, the training was performed with the Levenberg–Marquardt function (Marquardt 1963) using a back-propagation algorithm. The Levenberg–Marquardt function is a curve-fitting

Table 1 | Statistics of the input and output variables

	Water saturation, S (-)	Permeability, k (m^2)	Entry pressure, P_d (Pa)	Domain volume, V (m^3)	Pore size distribution, λ (-)	Viscosity ratio, μ_r (-)	Porosity, ϕ (-)	Density ratio, D_r (-)	Temperature, T (C)	Dynamic coefficient, τ (Pa s)
Maximum	9.96×10^{-1}	5.00×10^{-9}	1.50×10^{3}	1.57×10^{-3}	8.84	1.00×10^{3}	0.400	2.00	80.00	1.05×10^{11}
Minimum	1.05×10^{-1}	1.50×10^{-11}	3.75×10^{2}	3.27×10^{-4}	2.07	5.00×10^{-1}	0.32	0.50	20.00	1.18×10^{3}
Arithmetic average	4.78×10^{-1}	1.70×10^{-9}	7.78×10^{2}	9.41×10^{-4}	3.44	1.77×10^{2}	0.373	1.15	22.4	5.57×10^{9}
Standard deviation	2.57×10^{-1}	2.19×10^{-9}	4.29×10^{2}	2.42×10^{-4}	1.49	2.66×10^{2}	0.0311	0.374	9.43	1.89×10^{10}

function applied in nonlinear least squares problems. It optimizes the parameter of the model curve by minimizing the sum of the squares of the deviation from the empirical dependent variable. The back-propagation learning algorithm operates by iterative adjustment of the weights and biases in response to the error value between the predicted and the desired outputs. 'Tansig' and 'Purelin' transfer functions were used in this work. These transfer functions calculate a layer's output from its net input. While 'Tansig' is nonlinear, 'Purelin' is linear. For a network with a single hidden layer, 'Tansig' was used between the input and the hidden layers while 'Purelin' was used between the hidden and the output layer. For a network with a double hidden layer, 'Tansig' was used between the input and the hidden layers as well as between the first and the second hidden layers while 'Purelin' was used between the second hidden layer and the output.

Mean square error (MSE) was employed as the network default performance criterion relating the calculated outputs from the ANN to the actual target (dependent variable) in the training, validation and testing processes. In the simulation, pre-processing was performed using lines of code in the script with function 'mapminmax'. This function scales the inputs so that they fall into the range of -1 to 1.

In the training process, the epochs and goals serve as the stopping criteria of the number of iterations and the error tolerance, respectively. Epoch is the maximum number of times all of the training sets presented to the network while goal refers to the maximum error tolerance to be met by the developed network. Thus, the training stops if the error goal is met or the maximum number of epochs is attained. In this work, an epoch of 200 and a goal of zero were used. Different network configurations were constructed and each configuration differs in the number of hidden layers or neurons. The number of neurons was gradually increased for either single or double hidden layers. In this work, the representation of the layers in the ANN configurations is ANN [X-H1-Y] and ANN [X-H1-H2-Y] for single and double hidden layers, respectively. 'X' represents the input layer and its number refers to the number of independent variables, 'H1' and 'H2' represent the first and the second hidden layers, respectively, and their numbers represent the number of neurons in that layer. 'Y' is the output layer and its number represents the number of the dependent variable.

Linear and nonlinear regression models

For the purpose of comparisons with the performances of the different ANN configurations, multiple linear (LR) and nonlinear (NLR) regression models were investigated with the aid of MATLAB. Both regression models utilized the entire data set.

The LR was formulated for the nine independent variables against the dependent variable τ as shown in Equation (2)

$$\tau = b_0 + b_1(\chi_1) + b_2(\chi_2) + b_3(\chi_3) + b_4(\chi_4) + b_5(\chi_5) + b_6(\chi_6) + b_7(\chi_7) + b_8(\chi_8) + b9(\chi_9) \quad (2)$$

where $b_o, \ldots, b_9$ are the regression coefficients and $\chi_1, \ldots, \chi_9$ represent the independent variables. The regression coefficients for the LR were determined using the left division method (Gauss elimination and least square techniques) (Hanspal *et al.* 2013).

For the NLR of the independent variables, polynomials of various orders (Jain & Indurthy 2003) were used. The regression was implemented using the nonlinear fitting function in MATLAB to determine the vector of fit coefficients ($b_o, \ldots, b_9$) in the models listed below

$$\tau = b_0 + b_1(\chi_1)^{0.05} + b_2(\chi_2)^{0.05} + b_3(\chi_3)^{0.05} + b_4(\chi_4)^{0.05} + b_5(\chi_5)^{0.05} + b_6(\chi_6)^{0.05} + b_7(\chi_7)^{0.05} + b_8(\chi_8)^{0.05} + b_9(\chi_9)^{0.05}, \quad (3)$$

$$\tau = b_0 + b_1(\chi_1)^2 + b_2(\chi_2)^2 + b_3(\chi_3)^2 + b_4(\chi_4)^2 + b_5(\chi_5)^2 + b_6(\chi_6)^2 + b_7(\chi_7)^2 + b_8(\chi_8)^2 + b_9(\chi_9)^2, \quad (4)$$

$$\tau = b_0 + b_1(\chi_1)^3 + b_2(\chi_2)^3 + b_3(\chi_3)^3 + b_4(\chi_4)^3 + b_5(\chi_5)^3 + b_6(\chi_6)^3 + b_7(\chi_7)^3 + b_8(\chi_8)^3 + b_9(\chi_9)^3, \quad (5)$$

$$\tau = b_0 + b_1(\chi_1)^4 + b_2(\chi_2)^4 + b_3(\chi_3)^4 + b_4(\chi_4)^4 + b_5(\chi_5)^4 + b_6(\chi_6)^4 + b_7(\chi_7)^4 + b_8(\chi_8)^4 + b_9(\chi_9)^4. \quad (6)$$

ANN performance testing criteria

The performance of all ANNs were weighed with different statistical evaluations as demonstrated in Hanspal *et al.* (2013) using the following statistical analyses.

Sum square error

This describes the total deviation of the predicted values (S_{cal}) from the target values (S_{obs})

$$\mathrm{SSE} = \sum_{i=1}^{N} (S_{obs} - S_{cal})^2 \tag{7}$$

where N = total number of data points predicted, $S_{obs=}$ observed or target values of dynamic coefficient, τ and S_{cal} = predicted or calculated value of dynamic coefficient τ.

Average absolute relative error

This is the average of the relative errors in the prediction of a particular variable and it is expressed as a percentage. Lower values of average absolute relative error (AARE) indicate better model performance. It can be computed as follows:

$$\mathrm{AARE} = \frac{1}{N}\sum_{i=1}^{N}\left|\frac{S_{cal} - S_{obs}}{S_{obs}}\right| \times 100. \tag{8}$$

Nash-Sutcliffe efficiency coefficient (*E*)

The Nash-Sutcliffe efficiency coefficient is used to describe the accuracy of model outputs in relation to observed data. A value of E equal to 1 depicts a perfect match between observed data and outputs; therefore, the closer the model efficiency is to unity the more accurate the model. E is computed as follows:

$$E = 1 - \frac{\sum (S_{cal} - S_{obs})^2}{\sum (S_{obs} - \bar{S}_{obs})^2} \tag{9}$$

where $\bar{S}_{obs}$ = average observed dynamic coefficient τ in this work.

Pearson product moment coefficient of correlation (*R*)

This is a measure of the strength of linear dependence in the relationship between calculated and observed values of a modeled variable. Values of R equal to 1.0 indicate a perfect model. It is computed as follows:

$$R = \frac{\sum (S_{obs} - \bar{S}_{obs}) \times (S_{cal} - \bar{S}_{cal})}{\sqrt{\sum (S_{obs} - S_{obs})^2 \sum (S_{cal} - \bar{S}_{cal})^2}} \tag{10}$$

where $\bar{S}_{cal}$ = average calculated dynamic coefficient τ in this work.

Threshold statistics

The threshold statistic for a level of absolute relative error of $x\%$ from a particular model is a measure of consistency in the prediction errors (Jain & Ormsbee 2002). The threshold statistic can be computed as follows:

$$\mathrm{TS} = \frac{N_x}{N} \tag{11}$$

where N_x = number of data points predicted for which the average relative error is less than $x\%$. Larger values of threshold statistics (TS) indicate better model performance.

Mean squared errors

MSE measures the average of the squares of the errors between the observed value (S_{obs}) and the predicted or estimated value (S_{cal}). For N number of data points or cases, MSE can be obtained by averaging the sum square error (SSE) (see Equation (7))

$$\mathrm{MSE} = \frac{1}{N}\sum_{i=1}^{N} (S_{obs} - S_{cal})^2. \tag{12}$$

Prediction of domain scale dependency of τ–S relationships

Following the rigorous statistical evaluation of the models developed and described above, prediction of the effect of

domain size on the τ–S relationships was performed using the best-performing model. Separate data from independent experiments are predicted separately. To do this, the actual domain volume (V) of the experiment was increased by 10 or 20% and the corresponding τ was predicted as a function of saturation using the best-performing ANN.

RESULTS AND DISCUSSION

A computationally cost-effective and reliable ANN structure that predicts the domain scale dependency of $\tau - S$ relationships will serve a useful purpose in determining the significance of dynamic capillary pressure for two-phase flow systems. Our results aim to demonstrate this possibility. So, the results of training, validation and testing of the ANNs are discussed below. Also, the performances of the different ANN configurations together with the MVR models are compared on the bases of the different performance criteria. Scale dependency of $\tau - S$ relationships were then predicted for two-phase flow systems using the best-performing configuration.

ANN configurations

The training, validation and testing as well as the post-training regression analyses for different ANN configurations are shown in Figures 1 and 2 for ANN [9-13-15-1] and ANN [9-15-17-1], respectively. Figure 1(a) shows how the MSE reduces during training, validation and testing as the number of epoch increases. This eventually culminates in the optimal performance during validation at 108 epochs having approximately zero MSE value, i.e., 0.0023. This behavior shows that the network learns well as the number of epochs increase. The testing session shows acceptable MSE that is very close to zero as well. The post-training regression analysis (Figure 1(b)) shows how the LR line fits the data points. This regression line has a correlation coefficient (c) and slope (m) of 0.99 and 0.97, respectively, which are very close to 1. These show the reliability of the fit. In the figure, it can be observed that the target data cluster around the regression line in a way that shows reliable prediction. Similarly, the behavior of the network for ANN [9-15-17-1] is shown in Figure 2. The network exhibits similar behavior as discussed above. The learning improves

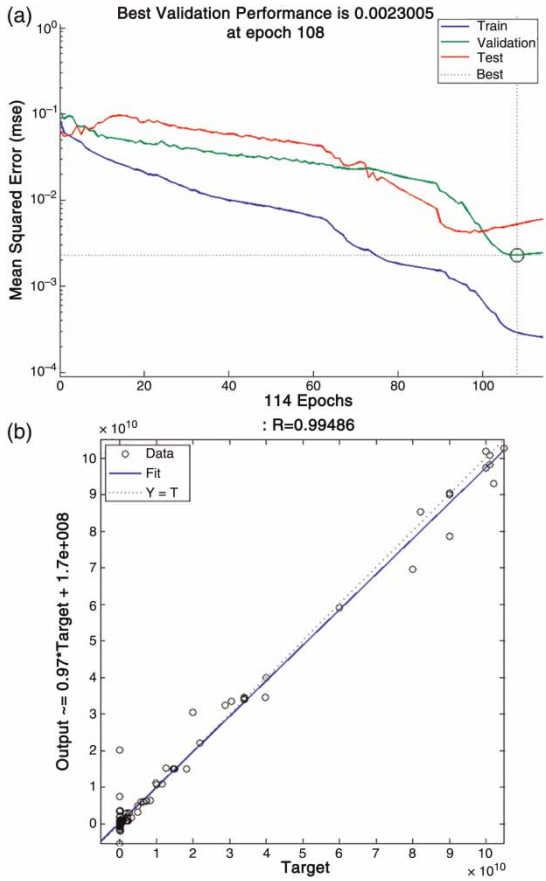

Figure 1 | (a) Training and (b) post-training regression analysis using ANN [9-13-15-1].

with the number of epochs for the training, validation and testing (Figure 2(a)). This is indicated by the reduction in the MSE values and the optimal MSE with validation occurs before the number of epochs reaches 51. In comparison to the behavior of ANN [9-13-15-1], shown in Figure 1(a), the testing and validation errors are larger in Figure 2(a), under the corresponding condition. The regression line for the ANN structure [9-15-17-1] is shown in Figure 2(b). The fit shows good c and m values of approximately 0.95 and 1.00, respectively. The regression analysis in Figure 2(b) shows that the cluster of the target data around the regression fit line is more scattered unlike that shown for ANN [9-13-15-1] (Figure 1(b)). This gives indication that ANN [9-13-15-1] may be more reliable than ANN [9-15-17-1]. However, the latter learns faster than the former.

The performances of various ANN configurations, in terms of the values of c and m of the regression line of fits

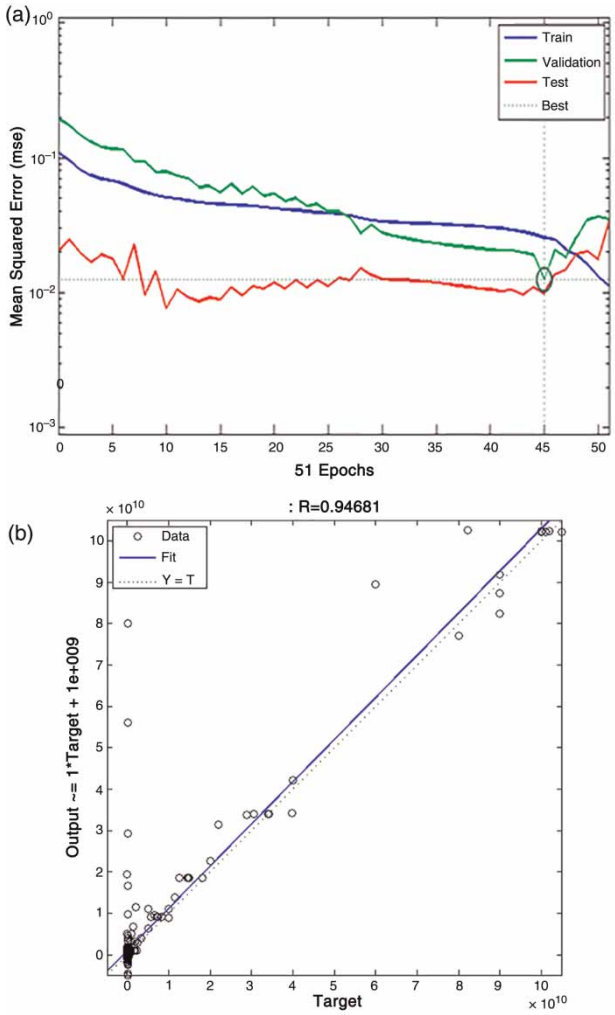

Figure 2 | (a) Training and (b) post-training regression analysis using ANN [9-15-17-1].

to the target data τ are listed in Table 2. As is well known, values of the slope m and correlation coefficient c closer to 1 indicate reliable prediction. From the table, it can be observed that the majority of the ANN configurations perform well as indicated by the high values of c and m. However, the two-hidden-layer models perform better than the single-hidden-layer models as they have the slope and correlation coefficient closer to 1 than the single-hidden-layer structure. In all, ANN [9-13-15-1] and ANN [9-15-17-1] appear to be leading in performance. However, the criteria listed in the 'ANN performance testing criteria' subsection are further employed in weighing the performance of all the models including the MVR models. In Table 2, the slope of the regression line obtained from

Table 2 | Slope and correlation coefficient for different artificial neural network configurations (single and double hidden layered artificial neural network structures)

S/N	ANN configurations	Slope (m)	Correlation coefficient (c)
1	9-2-1	0.7986	0.7986
2	9-3-1	0.8557	0.8557
3	9-4-1	0.925	0.925
4	9-5-1	0.8819	0.8819
5	9-7-1	0.8459	0.8459
6	9-9-1	0.9218	0.9218
7	9-10-1	0.8976	0.8976
8	9-2-2-1	0.881	0.881
9	9-3-2-1	0.8345	0.8345
10	9-2-3-1	0.8962	0.8962
11	9-5-3-1	0.9191	0.9191
12	9-7-5-1	0.9406	0.9406
13	9-9-7-1	0.9262	0.9262
14	9-10-8-1	0.9529	0.9529
15	9-10-10-1	0.9631	0.9631
16	9-11-13-1	0.9865	0.9865
17	9-13-15-1	0.9723	0.9949
18	9-15-17-1	1.0185	0.9468

ANN [9-15-17-1] is shown to be slightly greater than 1 (i.e., 1.02). This can be explained to mean slight overprediction of the target data by the model. This is also visible in Figure 2(b) where the line of fit is slightly above the best line of fit (i.e., $Y = T$). In contrast, Figure 1 shows that the regression line obtained from ANN [9-13-15-1] lies slightly below the best line of fit (i.e., $Y = T$) and hence, the slope is slightly below 1 (i.e., 0.97).

Figure 3 shows the plots of AARE for all ANN configurations, LR and NLR models. In comparison, AARE is generally low for the different ANN configurations while the LR and NLR generally have high AARE. The lower the AARE the better the performance (Hanspal *et al.* 2013). Thus, it seems that the ANNs perform better than the LR and NLR models. Among the ANN configurations, ANN [9-13-15-1] has the least AARE followed by ANN [9-11-13-1].

In Figure 4, the plots of the SSE similarly show that the SSE is generally higher for LR and NLR models. For the ANN structures, the ANN [9-13-15-1] configuration has the least SSE followed by ANN [9-11-13-1]. Comparison of the model output in relation to the target is described in terms

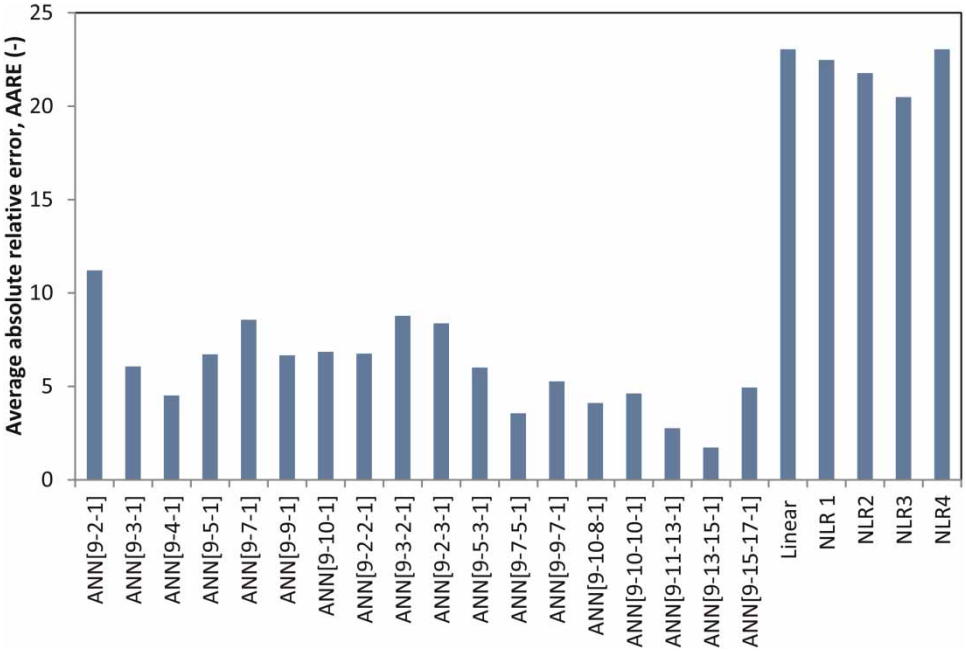

Figure 3 | AARE for ANN, LR and NLR models.

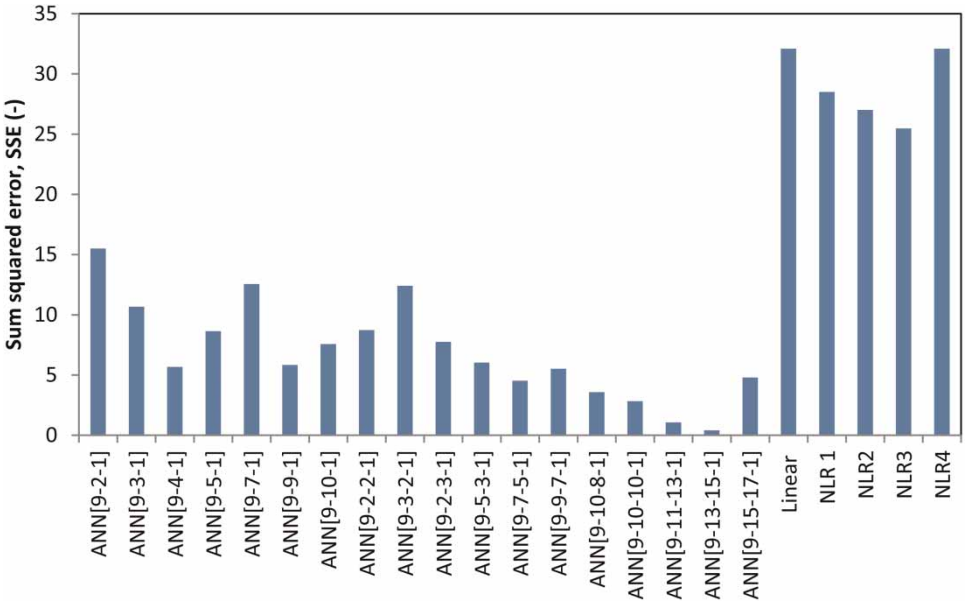

Figure 4 | SSE for ANN, LR and NLR models.

of Nash-Sutcliffe efficiency coefficient (E) depicted in Figure 5 for all the models. Again, it is visible that ANN [9-13-15-1] has the highest efficiency followed by ANN [9-11-13-1]. Also, TS for all the models show that ANN [9-13-15-1], ANN [9-11-13-1] and ANN [9-15-17-1] have the leading percentages. The plots are shown in Figure 6 for TS 5, TS 10, TS 25, TS 50 and TS 100. High values of TS imply good model performance.

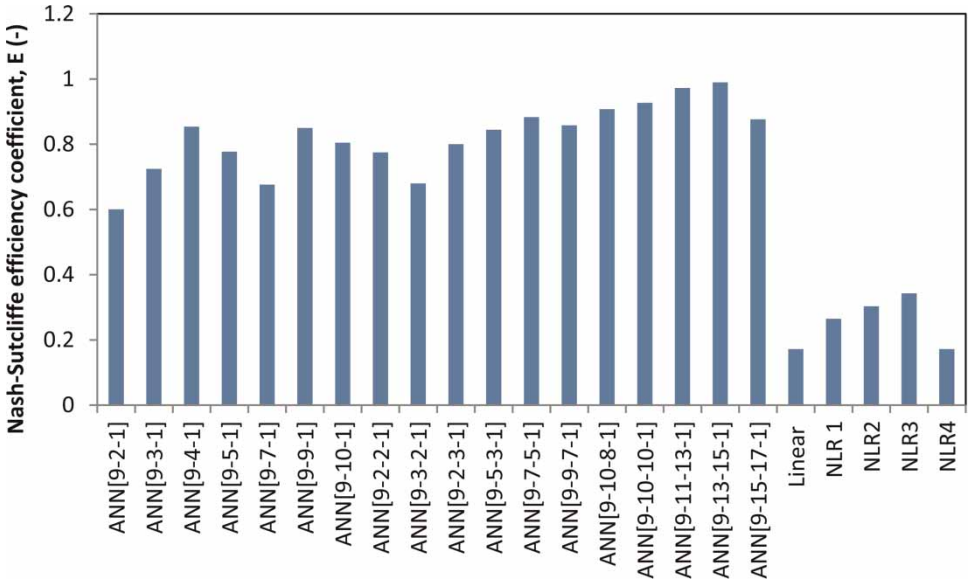

Figure 5 | Model output efficiency for ANN, LR and NLR models.

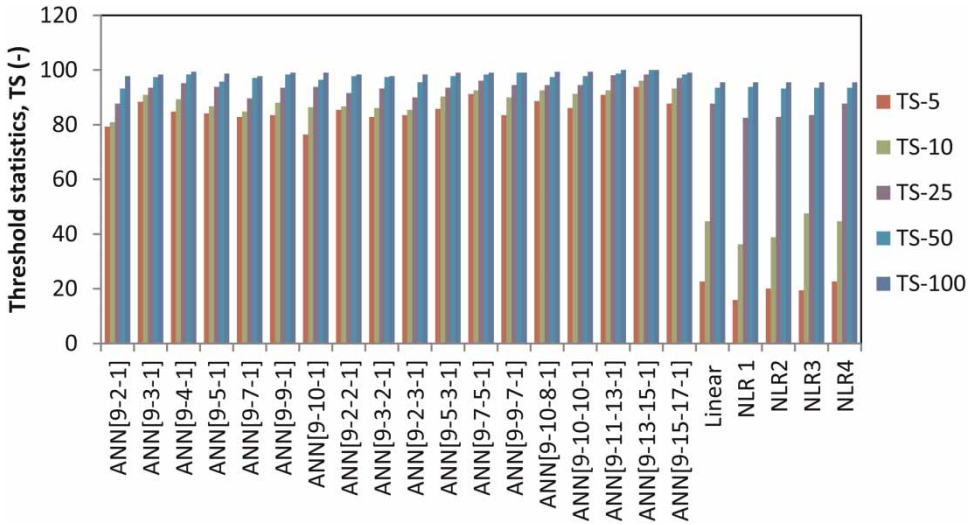

Figure 6 | TS for ANN, LR and NLR models.

From the above discussions, the performance criteria show that ANN structures have better reliability in predicting the two-phase flow parameters than MVR models (both linear and nonlinear). From the results, ANN [9-13-15-1] has shown the best performance.

Prediction of τ–S relationships

Results of the statistical analyses discussed in the 'ANN configurations' section compare the predicted output of the models to the actual target output (τ). The discussions in this section focus on the comparison of the actual $\tau - S$ relationships (target) to that predicted by some selected ANN, which include the best-performing model: ANN [9-13-15-1]. Figure 7 shows the plot of $\tau - S$ relationships using the entire data set in comparison with the prediction by ANN [9-13-15-1]. One can observe that the ANN structure has a good predictive ability of the $\tau - S$ relationships at both low and high saturation. Almost the entire $\tau - S$ data set are overlaid by the predicted values. In the figure,

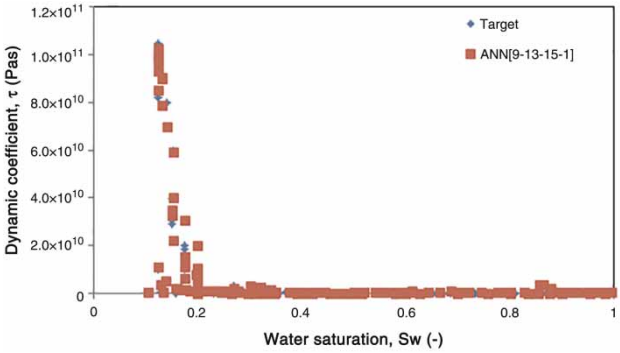

Figure 7 | Plots of the dynamic coefficient values from ANN structures output and target data against water saturation using ANN [9-13-15-1].

τ is shown to increase as the saturation reduces. From the start of the displacement of the wetting phase by the non-wetting phase, there exists only minimal change in τ as the saturation reduces. The trend, however, changes around the irreducible saturation where the τ value rises very steeply. This trend is widely reported in literature (Camps-Roach *et al.* 2010; Sakaki *et al.* 2010; Goel & O'Carroll 2011; Das & Mirzaei 2013). According to Das *et al.* (2007), increase in the magnitude of τ indicates increased deviation of the $P^c - S$ relationships from the equilibrium condition. Since the magnitude of τ becomes spectacularly large toward irreducible saturation, one can infer that the system properties at this region exhibit wider deviations from equilibrium.

Predictions of the $\tau - S$ relationships by ANN [9-15-17-1], ANN [9-10-10-1] and ANN [9-11-13-1] are shown in Figures 8–10, respectively. While these plots show good prediction of the $\tau - S$ relationships for the entire data set, they

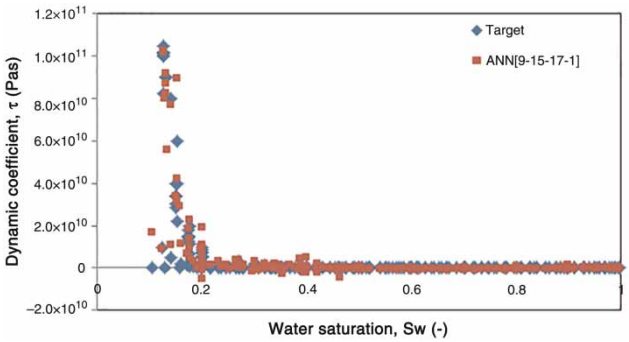

Figure 8 | Plots of the dynamic coefficient values from ANN structures output and target data against water saturation using ANN [9-15-17-1].

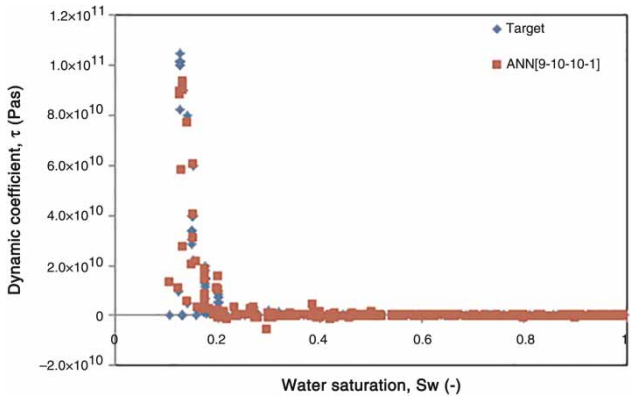

Figure 9 | Plots of the dynamic coefficient values from ANN structures output and target data against water saturation using ANN [9-10-10-1].

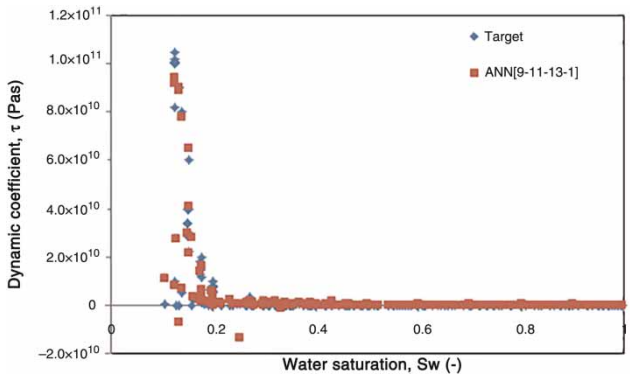

Figure 10 | Plots of the dynamic coefficient values from ANN structures output and target data against water saturation using ANN [9-11-13-1].

show more mismatches in comparison with Figure 7, especially at low water saturation or at high values of τ. However, ANN [9-11-13-1] and ANN [9-10-10-1] appear to predict better than ANN [9-15-17-1], having a lower number of mismatches especially at low water saturation.

Plots of the predictions of $\tau - S$ relationships by LR and NLR models are shown in Figures 11 and 12. The predictions by these models are less reliable, especially at low water saturation where the τ values are higher. The performances of these regression models are much less satisfactory in comparison to any of the ANN configurations with plots shown in Figures 7–10. This reveals the limitations of the regression models in the prediction of $\tau - S$ relationships for two-phase flow systems.

Judging from the results of the statistical analyses on the prediction of τ as well as the above models' performances on the prediction of $\tau - S$ relationships, one can conclude that

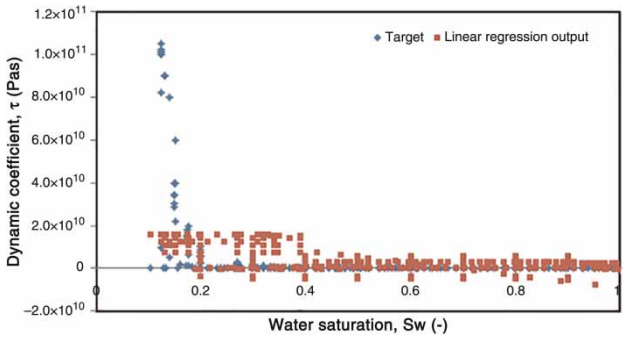

Figure 11 | Plots of the dynamic coefficient against the water saturation values for the entire data set and the predictions by LR structure.

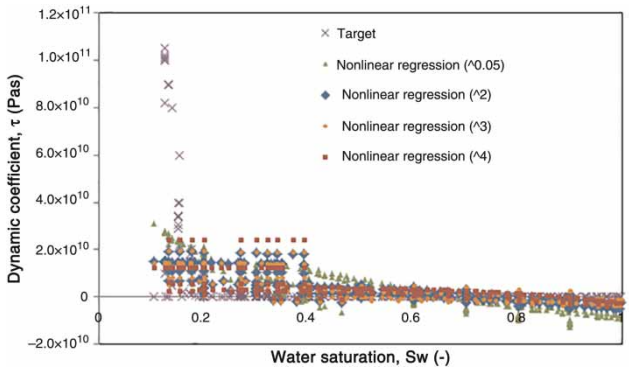

Figure 12 | Plots of the dynamic coefficient against the water saturation values for the entire data set and the predictions by NLR structures.

ANN [9-13-15-1] is the best structure among the models tested in this work. This conclusion is similar to that of Hanspal *et al.* (2013). They found that the regression models performed poorly in the prediction of the $\tau - S$ relationships and concluded that generally the regression models have much less predictive ability than ANN structures for two-phase flow system characteristics. In their work, the display of NLR models seems better than shown in Figure 12 of this work even though similar functions were used. This can be explained by the fact that they utilize only five independent variables in their work as different from the nine used in this work. Therefore, one can infer that the performance of the regression models becomes less reliable as the number of independent variables increases for two-phase flow systems.

Domain scale dependency of τ–S relationships

In the previous analyses and discussions, the ANN [9-13-15-1] structure is shown to be the best-performing network in the context of this work. In this section, the network is used to predict the domain scale dependency of $\tau - S$ relationships on the basis that the network is trained and validated. Separate data from different experiments are independently predicted. These include data from the literature as well as our in-house laboratory experiments.

Figures 13–15 display the results of the predictions. In the figures, τ for the original domain size is represented by two plots. One plot was obtained from the experimental data and the other was obtained from the ANN prediction of the original experimental data at the original domain scale (volume). These are labeled original volume (experiment) and the original volume (ANN) for the actual

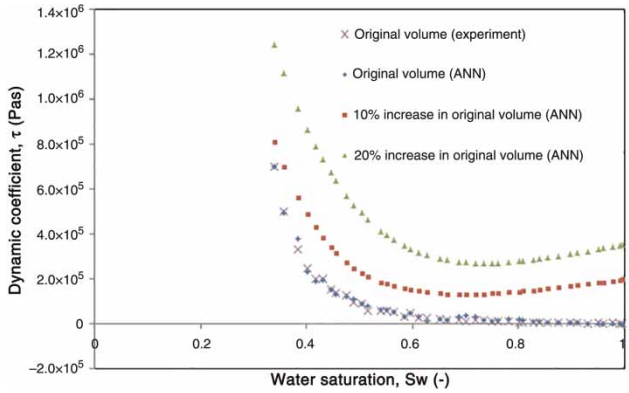

Figure 13 | Prediction of dynamic coefficient values against water saturation for the original, 10%, and 20% increase in domain size using the ANN [9-13-15-1]. Data for the original domain size were obtained from Das & Mirzaei (2012) where the oil viscosity is 200 cSt.

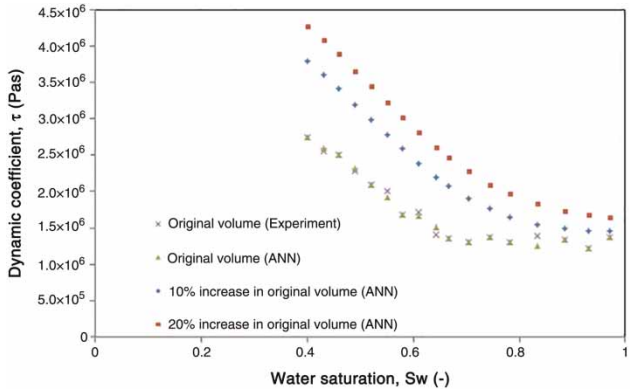

Figure 14 | Prediction of dynamic coefficient values against water saturation for the original, 10%, and 20% increase in domain size using ANN [9-13-15-1]. Data for original domain size were obtained from Goel & O'Carroll (2011) where the oil viscosity is 5 cSt.

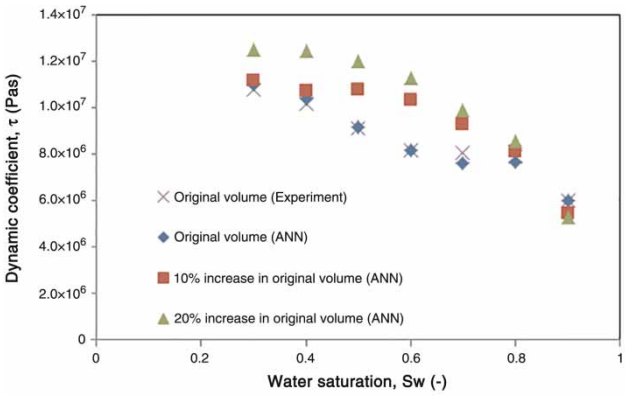

Figure 15 | Dynamic coefficient values against water saturation for the original, 10% and 20% increase in domain size using ANN [9-13-15-1]. Data for original domain size were obtained from our laboratory experiments (Abidoye & Das 2015) using methodology described by Das & Mirzaei (2012) but using an oil viscosity of 500 cSt.

experimental data and the ANN prediction, respectively. The other two plots in each of the figures are obtained when the domain scale (volume) is increased by 10 and 20%, respectively, and the corresponding $\tau - S$ relationships are predicted using ANN [9-13-15-1]. The results show that increasing the volume of the domain increases the magnitude of τ. This is shown in Figure 13. At 10% increase in original domain volume, $\tau - S$ curve lies higher than at the original domain size. This effect becomes greater at 20% increase in domain volume.

This trend points to an important observation in the literature about the $\tau - S$ dependency on the domain scale. Several authors have reported the same phenomenon (Dahle *et al.* 2005; Bottero *et al.* 2011a, b). Bottero *et al.* (2011a, b) found that there is a shift to higher values in the $\tau - S$ relationships as the scale goes from local measurements to higher averaging windows. Also, Dahle *et al.* (2005) using a bundle of tubes model reports this phenomenon with a greater effect of scale on $\tau - S$ relationships which is said to be proportional to the square of the length of the domain.

Furthermore, using the experimental results by Goel & O'Carroll (2011), increasing the domain volume shows an increase in the $\tau - S$ relationships. This is shown in Figure 14. The relationship for 10% increases in the domain size lies above the $\tau - S$ curve from the original experimental domain size. A 20% increase in the domain size also shows further rise in the $\tau - S$ relationships.

Finally, results from our laboratory for a higher viscosity ratio silicone oil-water system (500) were also tested using the ANN [9-13-15-1]. This is shown in Figure 15. It can be seen from the figure that the $\tau - S$ curve rises as the domain size increases. But the rise in this case is rather sluggish, especially at higher water saturation. This can be attributed to the high viscosity ratio (500) in this case. The original $\tau - S$ curve of Das & Mirzaei (2013) shown in Figure 13 uses a viscosity ratio of 200 and the work of Goel & O'Carroll (2011) uses a viscosity ratio of 5. Viscosity ratio refers to the ratio of the viscosity of the oil to that of the water.

As demonstrated above, the trend in $\tau - S$ as the domain size increases, which indicates the dependency of the dynamic effects in the system properties of two-phase flow systems on the media characteristics. Since increase in τ indicates increased deviation from equilibrium (Das *et al.* 2007), the domain size certainly impacts the dynamic P^c–S relationships in two-phase flow in the porous media. Judging from Equation (1), increasing the magnitude of τ implies two things. Provided the value of $P^{c,static}$ remains unaffected by domain scale, then the increase in the value of τ is influenced by increasing value of $P^{c,dyn}$ and/or decreasing value of the $\partial S/\partial t$. Thus, it may be rightly considered that $P^{c,dyn}$ increases as the domain scale increases. Similarly, it is plausible to consider that $\partial S/\partial t$ decreases as the domain scale increases which may be caused by the decreasing pressure gradient as the domain height or size increases. While the simultaneous impact of the changes, mentioned above, can cause the observed effects on τ, the ratio of their contribution may differ. Bottero *et al.* (2011a, 2011b) observe that the marginal change in pressure difference $(P^{c,dyn} - P^{c,static})$ with upscaled windows of observation is less significant. They attribute the change of τ with domain scale to the $\partial S/\partial t$, which decreases significantly as the domain size or length increases. Thus, $\partial S/\partial t$ plays significant role in the domain scale dependency of τ.

CONCLUSION

Application of an ANN for the prediction of the scale dependence of the dynamic capillary pressure effects in two-phase flow in porous media has been elaborately demonstrated.

Statistical analyses of the models tested showed that ANN configurations with double hidden layers outperformed those with single layers. Further comparison of the ANNs with LR and NLR models showed that ANNs have better prediction ability of the two-phase flow system characteristics.

Using the best-performing ANN structure (ANN [9-13-15-1]) in this work, the prediction of the domain size dependency for $\tau - S$ relationships reveals that the $\tau - S$ curve rises as the domain size increases in all the viscosity ratios tested. It was pointed out that the rate of change of saturation plays a more significant role in the domain scale dependency of τ.

Our findings showed the reliability and applicability of the ANN in characterizing and predicting the complex relationships for two-phase flow in porous media. Since the ANN system can be readily accessed and conveniently set up, it offers savings in cost and computational time in comparison to the flow-physics-based simulators.

ACKNOWLEDGEMENTS

The work in this paper was conducted in the framework of the Engineering and Physical Sciences Research Council (EPSRC), UK, project GR/S94315/01, 'micro-heterogeneity and temperature effects on dynamic capillary pressure–saturation relationships for two-phase flow in porous media'. A PhD studentship awarded to L. K. A. by the Petroleum Technology Development Fund (PTDF), Nigeria, is gratefully acknowledged. Comments of three anonymous referees which have helped to improve the paper are appreciated.

REFERENCES

Abidoye, L. K., Das, D. B. & Khudaida, K. J. 2015 Geological carbon sequestration in the context of two-phase flow in porous media: A review. *Critical Reviews in Environmental Science and Technology* doi:10.1080/10643389.2014.924184 (in press).

Ahmadi, M. A., Ebadi, M., Shokrollahi, M. & Javad, S. M. 2013 Evolving artificial neural network and imperialist competitive algorithm for prediction oil flow rate of the reservoir. *Applied Soft Computing* **13** (2), 1085–1098.

Amato, F., López, A., Peña-Méndez, E. M., Vaňhara, P., Hampl, A. & Havel, J. 2013 Artificial neural networks in medical diagnosis. *Journal of Applied Biomedicine* **11** (2), 47–58.

Bear, J. 2013 *Dynamics of Fluids in Porous Media*. Dover Publications Inc., New York.

Bottero, S., Hassanizadeh, S. M. & Kleingeld, P. J. 2011a From local measurements to an upscaled capillary pressure–saturation curve. *Transport in Porous Media* **88** (2), 271–291.

Bottero, S., Hassanizadeh, S. M., Kleingeld, P. J. & Heimovaara, T. J. 2011b Nonequilibrium capillarity effects in two-phase flow through porous media at different scales. *Water Resources Research* **47** (10), W10505.

Camps-Roach, G., O'Carroll, D. M., Newson, T. A., Sakaki, T. & Illangasekare, T. H. 2010 Experimental investigation of dynamic effects in capillary pressure: grain size dependency and upscaling. *Water Resources Research* **46** (8), W08544.

Dahle, H. K., Celia, M. A. & Hassanizadeh, S. M. 2005 Bundle-of-tubes model for calculating dynamic effects in the capillary-pressure-saturation relationship. *Transport in Porous Media* **58** (1–2), 5–22.

Danish, M. & Jacquin, C. 1983 Influence du contraste des viscosités sur les perméabilités relatives lors du drainage. Expérimentation et modélisation. *Rev. Inst. Franc. Pétrole* **33** (6), 723–733.

Das, D. B. & Mirzaei, M. 2012 Dynamic effects in capillary pressure relationships for two-phase flow in porous media: experiments and numerical analyses. *AIChE Journal* **58** (12), 3891–3903.

Das, D. B. & Mirzaei, M. 2013 Experimental measurement of dynamic effect in capillary pressure relationship for two-phase flow in weakly layered porous media. *AIChE Journal* **59** (5), 1723–1734.

Das, D. B., Mirzaei, M. & Widdows, N. 2006 Non-uniqueness in capillary pressure–saturation–relative permeability relationships for two-phase flow in porous media: Interplay between intensity and distribution of random micro-heterogeneities. *Chemical Engineering Science* **61** (20), 6786–6803.

Das, D. B., Gauldie, R. & Mirzaei, M. 2007 Dynamic effects for two-phase flow in porous media: fluid property effects. *AIChE* **53** (10), 2505–2520.

Das, D. B., Gill, B. S., Abidoye, L. K. & Khudaida, K. K. 2014 A numerical study of dynamic capillary pressure effect for supercritical carbon dioxide-water flow in porous domain. *AIChE Journal* **60** (12), 4266–4278, http://dx.doi.org/doi:10.1002/aic.14577.

Das, D. B., Thirakulchaya, T., Deka, L. & Hanspal, N. S. 2015 Artificial neural network to determine dynamic effect in capillary pressure relationship for two-phase flow in porous media with micro-heterogeneities. *Environmental Processes* **2** (1), 1–18.

Deka, L. & Quddus, M. 2014 Network-level accident-mapping: distance based pattern matching using artificial neural network. *Accident Analysis & Prevention* **65**, 105–113, http://dx.doi.org/doi:10.1016/j.aap.2013.12.001.

Diamantopoulos, E. & Durner, W. 2012 Dynamic nonequilibrium of water flow in porous media: a review. *Vadose Zone Journal* **11** (3), W03503.

Dullien, F. A. L., Allsop, H. A., Macdonald, I. F. & Chatzis, I. 1990 Wettability and immiscible displacement in pembina cardium sandstone. *Journal of Canadian Petroleum Technology* **29** (4), 63–74.

El Tabach, E., Lancelot, L., Shahrour, I. & Najjar, Y. 2007 Use of artificial neural network simulation metamodelling to assess groundwater contamination in a road project. *Mathematical and Computer Modelling* **45** (7), 766–776.

Gielen, T., Hassanizadeh, S. M., Leijnse, A. & Nordhaug, H. F. 2005 Dynamic effects in multiphase flow: a pore-scale network approach. In: *Upscaling Multiphase Flow in Porous Media* (D. B. Das & S. M. Hassanizadeh, eds). Springer, The Netherlands, pp. 217–236.

Goel, G. & O'Carroll, D. M. 2011 Experimental investigation of nonequilibrium capillarity effects: fluid viscosity effects. *Water Resources Research* **47** (9), W09507.

Hanspal, N. & Das, D. 2012 Dynamic effects on capillary pressure–saturation relationships for two-phase porous flow: implications of temperature. *AIChE Journal* **58** (6), 1951–1965.

Hanspal, N. S., Allison, B. A., Deka, L. & Das, D. B. 2013 Artificial neural network (ANN) modeling of dynamic effects on two-phase flow in homogenous porous media. *Journal of Hydroinformatics* **15** (2), 540–554.

Hassanizadeh, S. M. & Gray, W. G. 1993 Thermodynamic basis of capillary pressure in porous media. *Water Resources Research* **29** (10), 3389–3405. http://dx.doi.org/10.1029/93WR01495.

Hassanizadeh, S. M., Celia, M. A. & Dahle, H. K. 2002 Dynamic effect in the capillary pressure–saturation relationship and its impacts on unsaturated flow. *Vadose Zone Journal* **1** (1), 38–57.

Hill, D. J., Minsker, B. S., Valocchi, A. J., Babovic, V. & Keijzer, M. 2007 Upscaling models of solute transport in porous media through genetic programming. *Journal of Hydroinformatics* **9** (4), 251–266.

Ingham, D. B. & Pop, I. 2005 *Transport Phenomena in Porous Media III*. Elsevier Science, Oxford, UK.

Jain, A. & Indurthy, S. 2003 Comparative analysis of event-based rainfall-runoff modeling techniques – deterministic, statistical, and artificial neural networks. *Journal of Hydrologic Engineering* **8** (2), 93–98.

Jain, A. & Ormsbee, L. E. 2002 Short-term water demand forecast modeling techniques: conventional methods versus AI. *Journal-American Water Works Association* **94** (7), 64–72.

Joekar-Niasar, V. & Hassanizadeh, S. M. 2011 Effect of fluids properties on non-equilibrium capillarity effects: dynamic pore-network modeling. *International Journal of Multiphase Flow* **37** (2), 198–214.

Johnson, V. M. & Rogers, L. L. 2000 Accuracy of neural network approximators in simulation-optimization. *Journal of Water Resources Planning and Management* **126** (2), 48–56.

Kalaydjian, F. 1987 A macroscopic description of multiphase flow in porous media involving space-time evolution of fluid/fluid interface. *Transport in Porous Media* **6** (2), 537–552.

Kalaydjian, F. 1992 Effect of the flow rate on an imbibition capillary pressure curve – theory versus experiment. In: *Proceedings of the Society of the Core Analysts in Third European Core Analysis Symposium*, Paris, France, September 14–16, Gordon and Breach Science Publishers, Reading, UK.

Kalogirou, S. A. 2000 Applications of artificial neural-networks for energy systems. *Applied Energy* **67** (1–2), 17–35.

Karimpouli, S., Fathianpour, N. & Roohi, J. 2010 A new approach to improve neural networks' algorithm in permeability prediction of petroleum reservoirs using supervised committee machine neural network (SCMNN). *Journal of Petroleum Science and Engineering* **73** (3), 227–232.

Khashei, M. & Bijari, M. 2013 Fuzzy artificial neural network (p, d, q) model for incomplete financial time series forecasting. *Journal of Intelligent and Fuzzy Systems* **26** (2), 831–845.

Khudaida, K. J. & Das, D. B. 2014 A numerical study of capillary pressure–saturation relationship for supercritical carbon dioxide (CO_2) injection in deep saline aquifer. *Chemical Engineering Research and Design* **92** (12), 3017–3030. http://dx.doi.org/doi:10.1016/j.cherd.2014.04.020.

Kobayashi, K., Hinkelmann, R. & Helmig, R. 2008 Development of a simulation-optimization model for multiphase systems in the subsurface: a challenge to real-world simulation-optimization. *Journal of Hydroinformatics* **10** (2), 139–152.

Manthey, S., Majid Hassanizadeh, S. & Helmig, R. 2005 Macro-scale dynamic effects in homogeneous and heterogeneous porous media. *Transport in Porous Media* **58** (1–2), 121–145.

Marquardt, D. W. 1963 An algorithm for least-squares estimation of nonlinear parameters. *Journal of the Society for Industrial & Applied Mathematics* **11** (2), 431–441.

Mehta, H. B., Pujara, M. P. & Banerjee, J. 2013 Prediction of two phase flow pattern using artificial neural network. In: *International Conference on Chemical and Environmental Engineering (ICCEE'2013)*, 15–16 April 2013, Johannesburg, South Africa.

Mirzaei, M. & Das, D. B. 2007 Dynamic effects in capillary pressure–saturations relationships for two-phase flow in 3D porous media: implications of micro-heterogeneities. *Chemical Engineering Science* **62** (7), 1927–1947.

Mirzaei, M. & Das, D. B. 2013 Experimental investigation of hysteretic dynamic effect in capillary pressure-saturation relationship for two-phase flow in porous media. *AIChE Journal* **59** (10), 3958–3974.

Mounce, S. R., Mounce, R. B., Jackson, T., Austin, J. & Boxall, J. B. 2014 Pattern matching and associative artificial neural networks for water distribution system time series data analysis. *Journal of Hydroinformatics* **16** (3), 617–632.

Mueller, A. V. & Hemond, H. F. 2013 Extended artificial neural networks: incorporation of a priori chemical knowledge enables use of ion selective electrodes for in-situ measurement of ions at environmentally relevant levels. *Talanta* **117**, 112–118, http://dx.doi.org/doi:10.1016/j.talanta.2013.08.045.

O'Carroll, D. M., Abriola, L. M., Polityka, C. A., Bradford, S. A. & Demond, A. H. 2005a Prediction of two-phase capillary

pressure–saturation relationships in fractional wettability systems. *Journal of Contaminant Hydrology* **77** (4), 247–270.

O'Carroll, D. M., Phelan, T. J. & Abriola, L. M. 2005b Exploring dynamic effects in capillary pressure in multistep outflow experiments. *Water Resources Research* **41** (11), W11419.

Oung, O., Hassanizadeh, S. M. & Bezuijen, A. 2005 Two-phase flow experiments in a geocentrifuge and the significance of dynamic capillary pressure effect. *Journal of Porous Media* **8** (3), 247–257.

Rogers, L. L. & Dowla, F. U. 1994 Optimization of groundwater remediation using artificial neural networks with parallel solute transport modeling. *Water Resources Research* **30** (2), 457–481.

Sakaki, T., O'Carroll, D. M. & Illangasekare, T. H. 2010 Direct quantification of dynamic effects in capillary pressure for drainage–wetting cycles. *Vadose Zone Journal* **9** (2), 424–437.

Smiles, D. E., Vachaud, G. & Vauclin, M. 1971 A test of the uniqueness of the soil moisture characteristic during transient, nonhysteretic flow of water in a rigid soil. *Soil Science Society of America Journal* **35** (4), 534–539.

Spalding, D. B. 1981 A general purpose computer program for multi-dimensional one-and two-phase flow. *Mathematics and Computers in Simulation* **23** (3), 267–276.

Srinivasulu, S. & Jain, A. 2006 A comparative analysis of training methods for artificial neural network rainfall–runoff models. *Applied Soft Computing* **6** (3), 295–306.

Stauffer, F. 1978 Time dependence of the relations between capillary pressure, water content and conductivity during drainage of porous media. *Proceedings IAHR Symposium on Scale Effects in Porous Media*, pp. 766–776, Thessaloniki, 29 August–1 September, 1978, IAHR, Madrid.

Tian, S., Lei, G., He, S. & Yang, L. 2012 Dynamic effect of capillary pressure in low permeability reservoirs. *Petroleum Exploration and Development* **39** (3), 405–411.

Topp, G. C., Klute, A. & Peters, D. B. 1967 Comparison of water content-pressure head data obtained by equilibrium, steady-state, and unsteady-state methods. *Soil Science Society of America Journal* **31** (3), 312–314.

Wang, L. & Fu, K. 2008 *Artificial Neural Networks*. Wiley Online Library.

White, H. 1989 Learning in artificial neural networks: A statistical perspective. *Neural Computation* **1** (4), 425–464.

Wildenschild, D., Hopmans, J. W. & Simunek, J. 2001 Flow rate dependence of soil hydraulic characteristics. *Soil Science Society of America Journal* **65** (1), 35–48.

Yan, S. & Minsker, B. 2006 Optimal groundwater remediation design using an adaptive neural network genetic algorithm. *Water Resources Research* **42** (5), 1–14, http://dx.doi.org/doi:10.1029/2005WR004303.

Yurdakul, M. & Akdas, H. 2013 Modeling uniaxial compressive strength of building stones using non-destructive test results as neural networks input parameters. *Construction and Building Materials* **47**, 1010–1019.

Zhang, G., Eddy Patuwo, B. & Hu, M. Y. 1998 Forecasting with artificial neural networks. *International Journal of Forecasting* **14** (1), 35–62.

First received 20 July 2014; accepted in revised form 4 November 2014. Available online 16 December 2014